Computers and Structures 199 (2018) 18–33

Contents lists available at ScienceDirect

Computers and Structures

journal homepage: www.elsevier.com/locate/compstruc

Transient implicit wave propagation dynamics with overlapping finite elements

Ki-Tae Kim, Lingbo Zhang, Klaus-Jürgen Bathe *

Department of Mechanical Engineering, Massachusetts Institute of Technology, Cambridge, MA, USA

ARTICLE INFO

Article history:
Received 16 November 2017
Accepted 13 January 2018

Keywords:
Wave propagations
Multiple waves
Implicit time integration
Bathe method
Finite elements
Overlapping finite elements

ABSTRACT

We present novel overlapping finite elements used with the Bathe time integration method to solve transient wave propagation problems. The solution scheme shows two important properties that have been difficult to achieve in the numerical solution of general wave propagations: monotonic convergence of calculated solutions with decreasing time step size and a solution accuracy almost independent of the direction of wave propagation through the mesh. The proposed scheme can be efficiently used with irregular meshes. These properties make the scheme (the combined spatial and temporal discretizations) promising to solve general wave propagation problems in complex geometries involving multiple waves. A dispersion analysis is given and various example problems are solved to illustrate the performance of the solution scheme.

1. Introduction

The finite element method with direct time integration is widely employed to solve transient wave propagation problems. Using the traditional finite element solution approach, however, accurate solutions are difficult to obtain due to the dispersion and dissipation errors caused by the spatial and temporal discretizations, see for example Refs. [1–7]. Accurate solutions can only be obtained of rather simple problems, like one-dimensional problems with a single wave traveling through the domain. In this case, a uniform mesh and optimal time step size can be used. However, for geometrically complex problems, irregular meshes need in general be used and it is difficult to improve the solution accuracy by refining the mesh and decreasing the time step size, whichever spatial and time discretizations are used. For such irregular meshes, the solution accuracy depends on the propagation direction considered even when the wave is traveling through an isotropic medium. The traditional finite element method with direct time integration is, therefore, not very effective for the solution of general two- and three-dimensional wave propagation problems with waves propagating in different directions and at different wave speeds.

Considerable research efforts have focused on reducing the dispersion error of finite element solutions, see for example Refs. [8–12]. Also, the spectral element method can be used [13,14]. However, the above difficulties have not been overcome when considering complex geometries, anisotropic media, general boundary conditions and multiple waves traveling through the continuum.

The method of finite spheres, a meshless method, enriched for wave propagation problems can be used with the Bathe time integration scheme to solve wave propagation problems but *uniform* spatial discretizations need be used [15,16]. An important observation in Refs. [15,16] is that in the uniform spatial discretizations, a decrease in the time step size leads to a more accurate solution, which is what an analyst intuitively expects, and numerical anisotropy is almost negligible. These are important observations because by using the largest wave speed to establish the time step size, accurate solutions for multiple types of waves can be obtained *and* regardless of the propagation directions. The details of the mathematical analysis of the solution procedure and illustrative example solutions are given in Refs. [15,16].

However, the major difficulty in using the method of finite spheres, like other meshless methods, is the very expensive numerical integration for the construction of the mass and stiffness matrices [17–19]. The integration cost is clearly prohibitive for irregular discretizations using spheres, see Ref. [19]. For uniform discretizations, the numerical integration can be performed only once for a typical sphere and the result can then be reused [18], but this approach can of course not be employed when non-uniform spatial discretizations need be used. The high computational cost of the method impedes its wide practical use in industry.

* Corresponding author.
E-mail address: kjb@mit.edu (K.J. Bathe).

https://doi.org/10.1016/j.compstruc.2018.01.007
0045-7949/

Recently, we proposed a new paradigm of analysis using mostly traditional finite elements with some overlapping finite elements, like finite spheres [19–22]. We also developed novel overlapping finite elements and demonstrated that for static analysis, using these overlapping finite elements, the solution accuracy is almost insensitive to geometric distortions and the numerical integration is not very expensive compared to the use of traditional finite elements [22]. While we considered only static solutions, the use of overlapping finite elements has clearly also good potential for dynamic analyses.

In this paper, for the solution of transient wave propagation problems, we enrich the overlapping finite elements of Ref. [22] using trigonometric functions and use the Bathe time integration method because of its favorable dissipation properties [23,24]. The same approach has already been applied for use of a traditional finite element [25] and the method of finite spheres [15,16]. However, as already mentioned above, the use of the method of finite spheres is not efficient in general practical analyses because of the very expensive numerical integrations. For the traditional finite element enriched with trigonometric functions, the solution effort is more acceptable, although high, but the solution accuracy is not as desired because the predicted response sensitively depends on the directions of waves traveling through the mesh and fine meshes or high-order harmonic functions are required.

Our objective in this paper is to analyze the overlapping finite element enriched with trigonometric functions together with the Bathe time integration method and illustrate that the combined spatial and time discretization scheme can be used to solve wave propagations in complex geometries using regular or irregular meshes. Hence, as we also demonstrate, the element can be used with the new paradigm of finite element solutions for CAD.

In the next section, we formulate the overlapping finite element for transient wave propagation problems. Then, in Section 3, we study the dispersion properties of the proposed scheme. Thereafter, in Section 4, we provide the calculated solutions of various wave propagation problems to illustrate the capability of the solution scheme. We focus on showing that even when using irregular meshes good results are obtained. Finally, we give the conclusions of our research in Section 5.

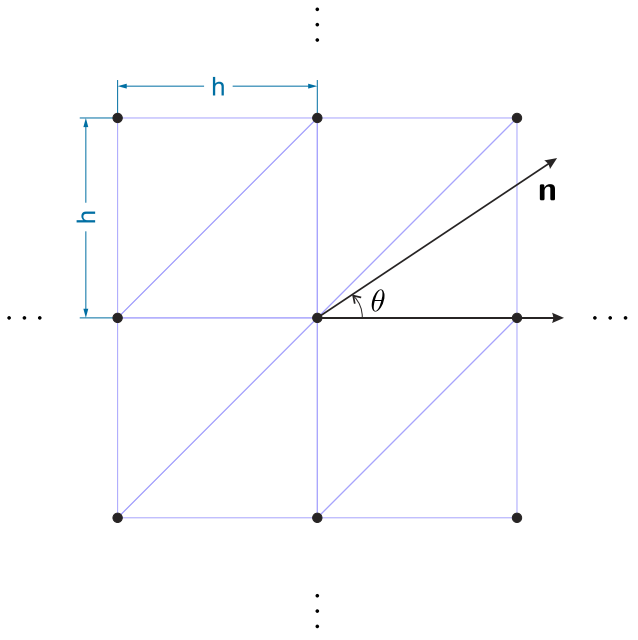

Fig. 1. Uniform mesh and propagation angle of a sinusoidal plane wave.

2. Spatial approximation scheme

In the new paradigm of finite element analysis, the global analysis domain is discretized by traditional finite elements (that do not overlap) and finite elements that overlap [20,21]. For every overlap region, the solution variable u is approximated as [19,22]

$$u \approx u_h = \sum_{I=1}^{q} h_I \psi_I = \sum_{I=1}^{q} h_I \sum_{J \in \mathcal{N}_I} \hat{\varphi}_J^I \sum_{n \in \mathfrak{I}_J} p_n a_{Jn} \tag{1}$$

where q is the number of nodes in the overlap region, h_I is the shape function used in the traditional finite element [26], ψ_I is the local field of the overlapping element I, $\mathcal{N}_I$ is the set of nodes located in the overlapping element I, $\hat{\varphi}_J^I$ is a partition of unity function, $\mathfrak{I}_J$ is an index set and p_n is a set of local basis functions (e.g., a polynomial for elliptic problems) which span the local approximation space V_J^h with the corresponding coefficient of node J. It is important to note that the function $\hat{\varphi}_J^I$ is a polynomial and hence the computational cost for establishing the stiffness and mass matrices is not high.

For the solution of two-dimensional wave propagation (hyperbolic) problems, the bi-linear polynomials and trigonometric functions (used like polynomials) are employed for the local approximation space, i.e., at node J we use

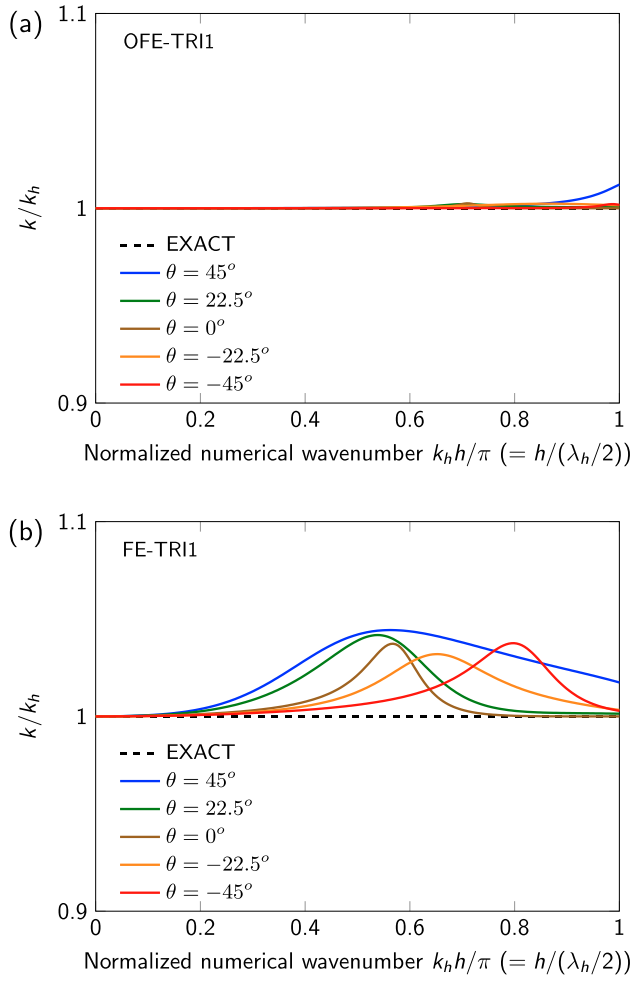

Fig. 2. Dispersion properties of (a) OFE-TRI1 and (b) FE-TRI1 discretizations for various propagation angles.

$$V_J^h = \text{span}\left\{ \begin{array}{c} 1, x, y, xy, \\ \cos\left(\frac{2\pi x}{\lambda_x}\right), \sin\left(\frac{2\pi x}{\lambda_x}\right), \cos\left(\frac{2\pi y}{\lambda_y}\right), \sin\left(\frac{2\pi y}{\lambda_y}\right), \\ \cos\left(\frac{2\pi x}{\lambda_x}+\frac{2\pi y}{\lambda_y}\right), \sin\left(\frac{2\pi x}{\lambda_x}+\frac{2\pi y}{\lambda_y}\right), \cos\left(\frac{2\pi x}{\lambda_x}-\frac{2\pi y}{\lambda_y}\right), \sin\left(\frac{2\pi x}{\lambda_x}-\frac{2\pi y}{\lambda_y}\right), \\ \ldots, \\ \cos\left(\frac{2\pi p x}{\lambda_x}\right), \sin\left(\frac{2\pi p x}{\lambda_x}\right), \cos\left(\frac{2\pi p y}{\lambda_y}\right), \sin\left(\frac{2\pi p y}{\lambda_y}\right), \\ \cos\left(\frac{2\pi p x}{\lambda_x}+\frac{2\pi p y}{\lambda_y}\right), \sin\left(\frac{2\pi p x}{\lambda_x}+\frac{2\pi p y}{\lambda_y}\right), \cos\left(\frac{2\pi p x}{\lambda_x}-\frac{2\pi p y}{\lambda_y}\right), \sin\left(\frac{2\pi p x}{\lambda_x}-\frac{2\pi p y}{\lambda_y}\right) \end{array} \right\} \tag{2}$$

where x and y are the Cartesian coordinates, λ_x and λ_y are the fundamental wavelengths in the x- and y-directions, respectively, and p is the degree of the trigonometric functions used. Hence the number of degrees of freedom per node is 12, 20, 28 when $p = 1, 2, 3$, respectively.

In a one-dimensional wave propagation, the local approximation space is, for node J,

$$V_J^h = \text{span}\left\{1, x, \cos\left(\frac{2\pi x}{\lambda_x}\right), \sin\left(\frac{2\pi x}{\lambda_x}\right), \ldots, \cos\left(\frac{2\pi p x}{\lambda_x}\right), \sin\left(\frac{2\pi p x}{\lambda_x}\right)\right\}. \tag{3}$$

Note that in the local approximation space, the polynomials are included to satisfy linear consistency, ensuring that the approximation can reproduce the linear field (e.g., rigid body displacements and constant strain states). For some experiences using such functions see, for example, Refs. [15,16,25,27].

In this study, we use $\lambda_x = \lambda_y = 2h$ where h is the typical size of overlap region and mainly focus on the use of $p = 1$. Of course, the use of a higher degree functions gives a better solution accuracy for a given mesh, but the solution is also computationally more costly [15,25].

3. Dispersion analysis

Following the approach given in Ref. [16], we investigate in this section the dispersion properties when solving the standard two-dimensional wave equation with the overlapping finite elements and the Bathe time integration scheme. We compare the results obtained to those when using the traditional finite elements enriched for wave propagation problems [25]. We first consider the dispersion errors caused by only the spatial discretization, and then analyze the additional effects resulting from the temporal discretization using the Bathe implicit time integration.

The wave equation is given by

$$\nabla^2 u - \frac{1}{c^2}\frac{\partial^2 u}{\partial t^2} = 0 \tag{4}$$

where t is time, ∇^2 is the Laplace operator and c is the wave propagation velocity. A basic sinusoidal plane wave solution to this equation in a fixed Cartesian coordinate system is given by

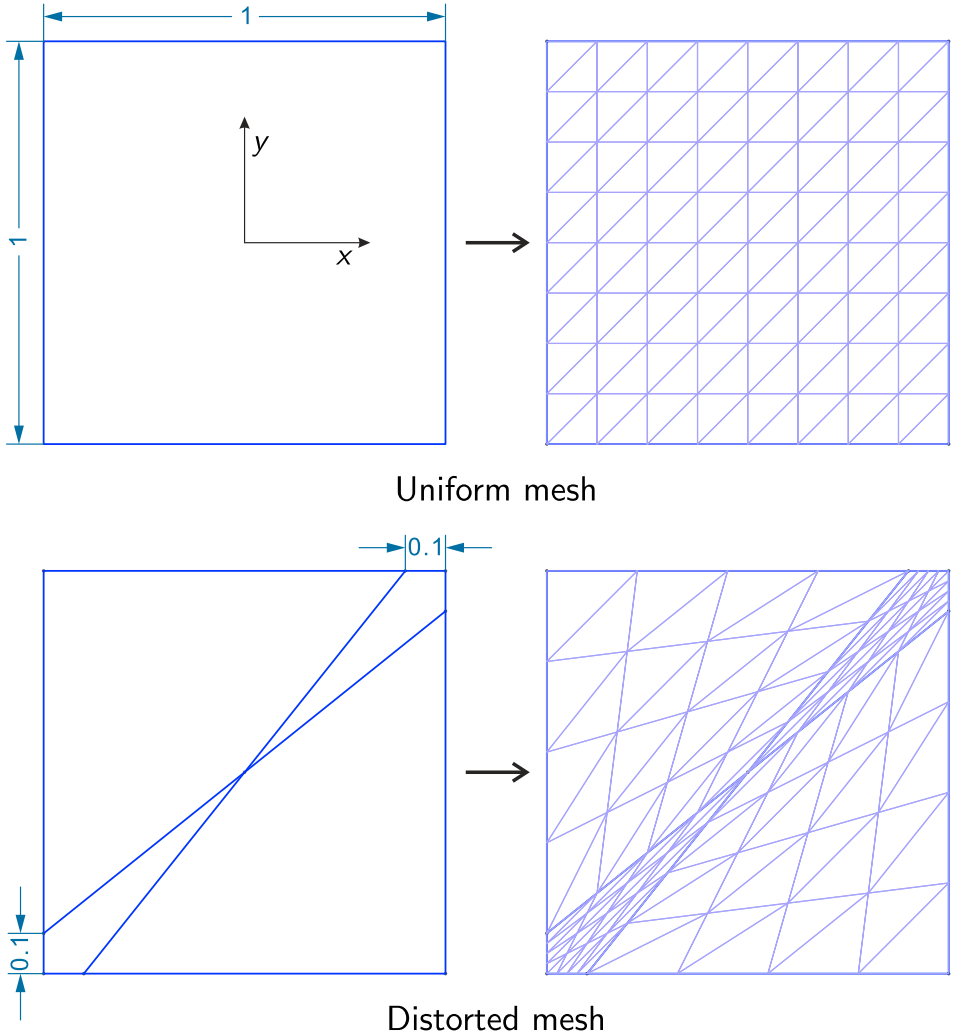

Fig. 3. Uniform and distorted meshes used for the simple problem for which the exact solution is $u = \sin(2\pi x)$; $h = 1/N$ where N is the number of elements along each side.

$$u = Ae^{i(k\mathbf{n}\cdot\mathbf{x}-\omega t)} \tag{5}$$

where A is the amplitude, k is the wave number, $\mathbf{n}$ is a unit vector in the direction of wave propagation, $\mathbf{x}$ is a position vector measured from the origin of the Cartesian coordinate system, ω is the angular frequency and $i = \sqrt{-1}$. Note that the analytical solution is non-dispersive, i.e.,

$$c^2 = \left(\frac{\omega}{k}\right)^2. \tag{6}$$

3.1. Spatial discretization error

We consider the time independent form of the wave equation, the Helmholtz equation, given as

$$\nabla^2 u + k^2 u = 0 \tag{7}$$

with a plane wave solution

$$u = Ae^{ik\mathbf{n}\cdot\mathbf{x}}. \tag{8}$$

The overlapping finite element discretization of the variational form of Eq. (7) yields, without considering boundary conditions,

$$\mathbf{Ka} - (kh)^2\mathbf{Ma} = \mathbf{0} \tag{9}$$

where $\mathbf{K}$, $\mathbf{M}$ and $\mathbf{a}$ are the corresponding dimensionless stiffness and consistent mass matrices and the vector of unknown coefficients, respectively.

For the dispersion analysis, we consider a uniform mesh which is translationally-invariant, see Fig. 1. Using the same n_p local basis functions for the local approximation space at each node, the coefficient vectors $\mathbf{a}_I$ associated with nodes I, $I = 1, 2, \ldots$, can be assumed of the form

$$\mathbf{a}_I = \hat{\mathbf{a}}e^{ik_h\mathbf{n}\cdot\mathbf{x}_I} \tag{10}$$

where $\hat{\mathbf{a}}$, k_h and $\mathbf{x}_I$ are the amplitude vector of order n_p, the numerical wave number and the nodal position vector, respectively. Substituting from Eq. (10) into Eq. (9) gives, after canceling the common factor, the same equation for all nodes, which can be written as

$$(\mathbf{D}_{\text{stiff}} - (kh)^2\mathbf{D}_{\text{mass}})\hat{\mathbf{a}} = \mathbf{0} \tag{11}$$

where $\mathbf{D}_{\text{stiff}}$ and $\mathbf{D}_{\text{mass}}$ are both Hermitian matrices of order $n_p \times n_p$. The condition for the existence of nontrivial solutions to Eq. (11) is

$$\det(\mathbf{D}_{\text{stiff}} - (kh)^2\mathbf{D}_{\text{mass}}) = 0. \tag{12}$$

The solution to this equation provides a relation between the values of kh and $k_h h$.

We also apply the same approach to the scheme discussed in Ref. [25], i.e. the triangular traditional finite element enriched with trigonometric functions of degree $p = 1$.

Fig. 2 shows the dispersion properties of the overlapping finite elements with the bilinear polynomials and the first degree trigonometric functions (OFE-TRI1) and of the traditional finite elements enriched with the first degree trigonometric functions (FE-TRI1). We see that the OFE-TRI1 discretization has practically no dispersion for the wave modes with $k_h h/\pi \leqslant 0.8$ regardless of the propagation direction. For the wave modes with $0.8 < k_h h/\pi \leqslant 1$, the dispersion errors depend on the propagation direction, but the errors are small. On the other hand, these observations are not applicable to the FE-TRI1 scheme, for which the dispersion errors are quite large. To obtain better results higher-order harmonic functions need to be included which however increases the computational complexities [25].

To illustrate the performance of the methods in uniform and distorted meshes, we solve a simple problem in the domain $V = [0,1] \times [0,1]$ for which the exact solution is $u = \sin(2\pi x)$, see Fig. 3. Fig. 4 shows the L^2 relative error norm e_r, defined by

$$e_r = \sqrt{\frac{\int_V (u - u_h)^2 \mathrm{d}V}{\int_V u^2 \mathrm{d}V}}, \tag{13}$$

of the solutions when using the OFE-TRI1 and FE-TRI1 discretizations with uniform and distorted meshes. As expected from the dispersion properties shown in Fig. 2, the OFE-TRI1 discretization with all the uniform meshes considered gives solutions with $\log_{10} e_r \leqslant -3$, while using the FE-TRI1 discretization, solutions with $\log_{10} e_r \leqslant -3$ are obtained only when the uniform meshes are used with $h = 1/64, 1/32$ ($\log_{10} h = -1.8, -1.5$), see Fig. 4.

When the distorted mesh shown in Fig. 3 is used, to have a solution with $\log_{10} e_r < -3$, the OFE-TRI1 discretization with all the distorted meshes considered can be used, but a very fine mesh is required when using the FE-TRI1 discretization, see Fig. 4.

3.2. Additional effects introduced by the Bathe time integration

Temporal discretizations using time integration methods result in period elongations and amplitude decays [26]. Period elongations lead to errors in the phase velocity (dispersion errors) and amplitude decays result in attenuations of the wave modes (dissipation errors). In this section, we analyze these additional numerical effects when using the Bathe implicit time integration.

We consider the overlapping finite element wave equation

$$\mathbf{M}\ddot{\mathbf{a}} + \left(\frac{c}{h}\right)^2\mathbf{Ka} = \mathbf{0} \tag{14}$$

where an overdot denotes time derivative. Using the translationally-invariant uniform mesh shown in Fig. 1 with Eq. (10), the above equation becomes

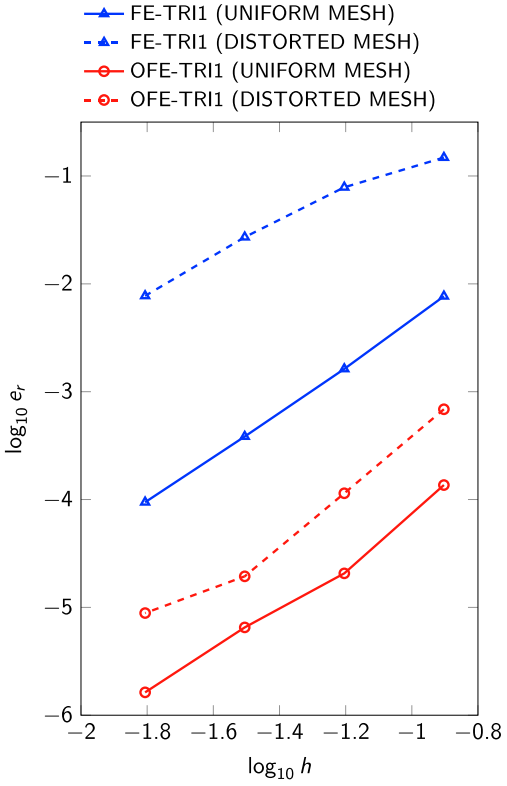

Fig. 4. The L^2 relative error norms of the solutions to the simple problem when using FE-TRI1 and OFE-TRI1 discretizations.

$$\mathbf{D}_{\text{mass}}\ddot{\hat{\mathbf{a}}} + \left(\frac{c}{h}\right)^2 \mathbf{D}_{\text{stiff}}\hat{\mathbf{a}} = \mathbf{0}. \tag{15}$$

Note that the amplitude vector $\hat{\mathbf{a}}$ is now a function of time. For the analysis, we perform a change of basis from the amplitude vector to the basis of eigenvectors of the following eigenproblem:

$$\mathbf{D}_{\text{stiff}}\boldsymbol{\varphi} = \lambda^2 \mathbf{D}_{\text{mass}}\boldsymbol{\varphi}. \tag{16}$$

Using

$$\hat{\mathbf{a}}(t) = \boldsymbol{\Phi}\mathbf{x}(t) \tag{17}$$

where the columns in $\boldsymbol{\Phi}$ are the $\mathbf{D}_{\text{mass}}$-orthonormalized eigenvectors $\boldsymbol{\varphi}_1, \ldots, \boldsymbol{\varphi}_{n_p}$, and substituting for $\hat{\mathbf{a}}$ into Eq. (15) we have

$$\ddot{\mathbf{x}} + \left(\frac{c}{h}\right)^2 \boldsymbol{\Lambda}^2 \mathbf{x} = \mathbf{0} \tag{18}$$

where $\boldsymbol{\Lambda}^2$ is a diagonal matrix listing the eigenvalues $\lambda_1, \ldots, \lambda_{n_p}$. To ascertain the dispersion and amplitude decay properties, we can now focus on a typical row of Eq. (18) which may be written as

$$\ddot{x} + \gamma^2 x = 0 \tag{19}$$

where $\gamma = c\lambda/h$.

Using the Bathe time integration scheme [23], we obtain the following relationship

$$\begin{bmatrix} {}^{t+\Delta t}\ddot{x} \\ {}^{t+\Delta t}\dot{x} \\ {}^{t+\Delta t}x \end{bmatrix} = \mathbf{A} \begin{bmatrix} {}^{t}\ddot{x} \\ {}^{t}\dot{x} \\ {}^{t}x \end{bmatrix} \tag{20}$$

where

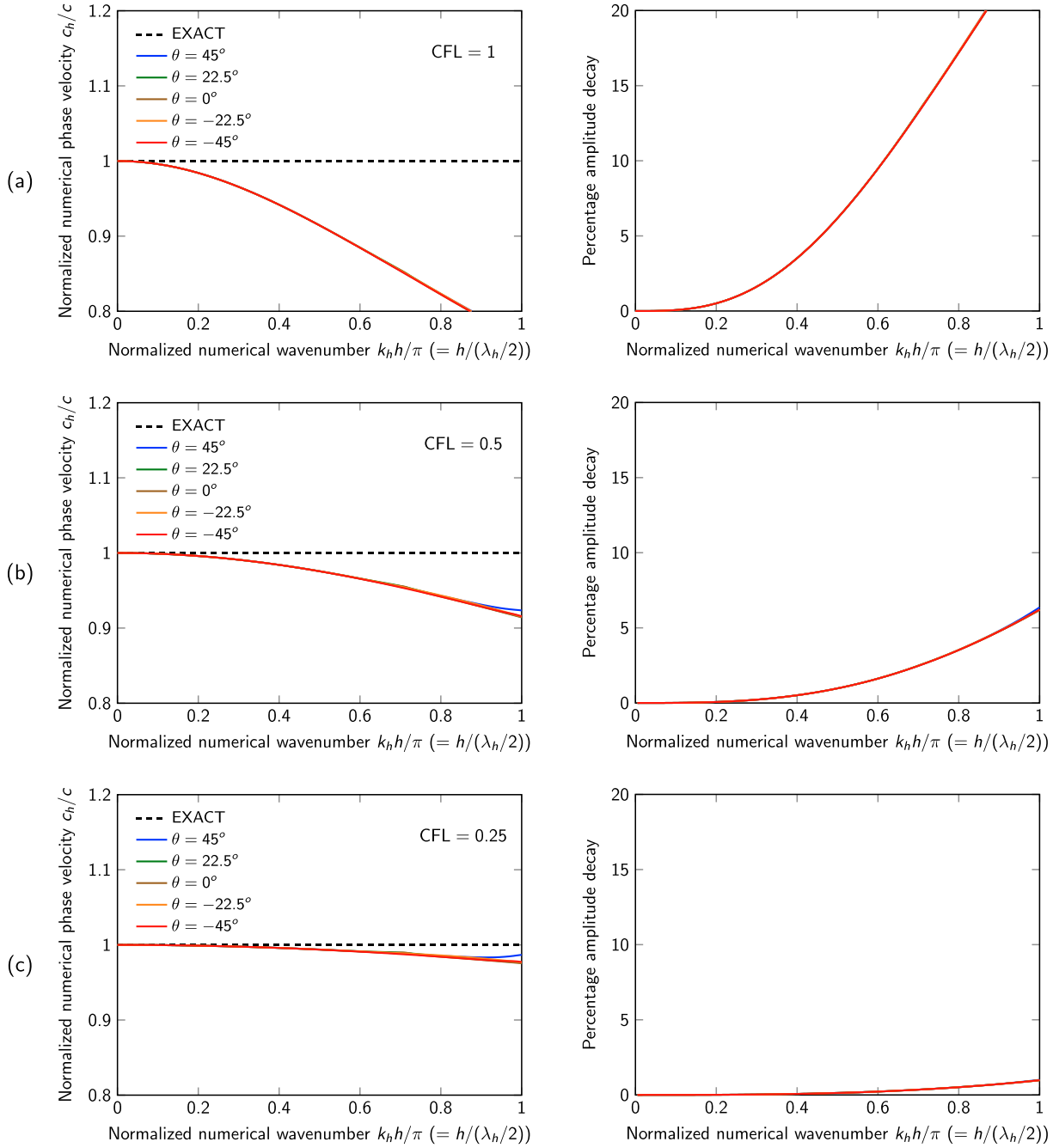

Fig. 5. Dispersion (left) and dissipation (right) properties of OFE-TRI1 scheme for various propagation angles: when (a) CFL = 1, (b) CFL = 0.5 and (c) CFL = 0.25.

$$\mathbf{A}=\frac{1}{\beta_1\beta_2}\begin{bmatrix} -28\gamma^2\Delta t^2 & \gamma(-144\gamma\Delta t+5\gamma^3\Delta t^3) & -\gamma^2(144-19\gamma^2\Delta t^2) \\ -4\Delta t(-12+\gamma^2\Delta t^2) & 144-47\gamma^2\Delta t^2 & \gamma^2\Delta t(-96+\gamma^2\Delta t^2) \\ 28\Delta t^2 & \Delta t(144-5\gamma^2\Delta t^2) & 144-19\gamma^2\Delta t^2 \end{bmatrix} \tag{21}$$

with $\beta_1 = 16+\gamma^2\Delta t^2$ and $\beta_2 = 9+\gamma^2\Delta t^2$. Note that the characteristic polynomial of the matrix **A** is

$$p_A(\eta) = \eta^3 - \frac{288-94\gamma^2\Delta t^2}{144+25\gamma^2\Delta t^2+\gamma^4\Delta t^4}\eta^2 + \frac{144+25\gamma^2\Delta t^2}{144+25\gamma^2\Delta t^2+\gamma^4\Delta t^4}\eta \tag{22}$$

and it can be found from $p_A(\eta_i)=0,\ i=1,2,3$, that there are two complex conjugate eigenvalues, η_1, η_2, which satisfy $|\eta_1|, |\eta_2| \leqslant 1$, and a zero eigenvalue, $\eta_3 = 0$, of **A**.

The recursive use of Eq. (20) with the equilibrium equation (19) gives

$${}^{t+2\Delta t}x - \frac{288-94\gamma^2\Delta t^2}{144+25\gamma^2\Delta t^2+\gamma^4\Delta t^4}{}^{t+\Delta t}x + \frac{144+25\gamma^2\Delta t^2}{144+25\gamma^2\Delta t^2+\gamma^4\Delta t^4}{}^{t}x = 0. \tag{23}$$

By comparing this equation with the equation $p_A(\eta)=0$, we note that the discrete solution to the above equation is of the form

$$x_h = c_1 e^{(-\xi_h+i)\omega_h t_h} + c_2 e^{(-\xi_h-i)\omega_h t_h} \tag{24}$$

where c_1 and c_2 are undetermined coefficients, ξ_h is a numerical damping ratio, ω_h is the numerical angular frequency and t_h is the discretized time. From this solution, we can obtain the relation between the numerical wave number k_h and the numerical angular

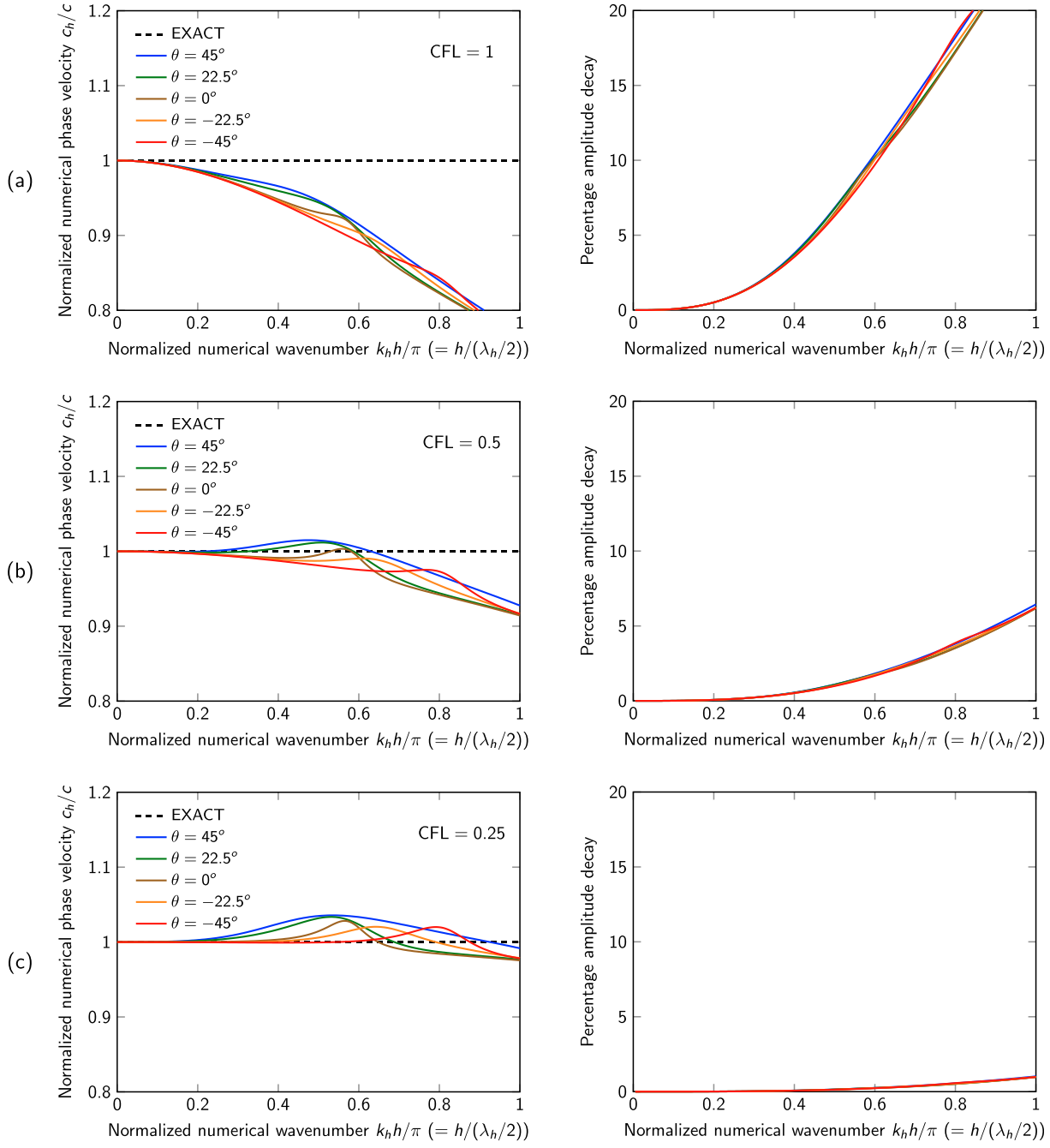

Fig. 6. Dispersion (left) and dissipation (right) properties of FE-TRI1 scheme for various propagation angles: when (a) CFL = 1, (b) CFL = 0.5 and (c) CFL = 0.25.

frequency ω_h as a function of the CFL number defined as $\text{CFL} = c\Delta t/h$. This number represents physically the ratio of the traveled length, $c\Delta t$, in the continuum per time step over the element length h. The percentage amplitude decay is calculated using

$$\text{Percentage amplitude decay} = (1 - e^{-2\pi\xi_h}) \times 100. \quad (25)$$

Fig. 5 shows the dispersion errors and the percentage amplitude decays of wave modes for various propagation angles when using the OFE-TRI1 discretization with the Bathe time integration (denoted by OFE-TRI1 scheme). It is important to note that practically all wave modes with $k_h h/\pi \leqslant 1$ monotonically converge to the exact wave modes when decreasing the CFL number and the accuracy does not depend on the propagation direction. This is not seen for the use of the FE-TRI1 discretization with the Bathe time integration (denoted by FE-TRI1 scheme) as shown in Fig. 6. The phase velocity shows a significant error, and this error depends on the direction considered, even when using CFL = 0.25.

We also observed this characteristic when using the method of finite spheres with the bi-linear polynomials and the trigonometric functions and the Bathe time integration scheme, denoted as the MFS-TRI scheme. In practical analyses, however, the MFS-TRI scheme is very expensive to use because of the computational cost when the nodes are distributed irregularly. Since the partition of unity function used in the OFE-TRI scheme is *a polynomial*, the computational effort in the OFE-TRI scheme is much smaller.

4. Numerical examples

In the previous section, we analyzed mathematically the important properties of the OFE-TRI1 scheme. The result is however valid only for the uniform mesh considered. Our objective in this section is to illustrate the important properties of the OFE-TRI1 scheme in both structured (regular) meshes and unstructured (irregular) meshes through numerical examples, and then show that the scheme can be used effectively with the meshing procedure proposed in Refs. [20,21].

We first consider scalar wave propagations in one- and two-dimensional media. Then we solve Lamb's problem [28] where different waves propagate in a semi-infinite elastic medium. Finally we solve a problem with transmitted and reflected waves.

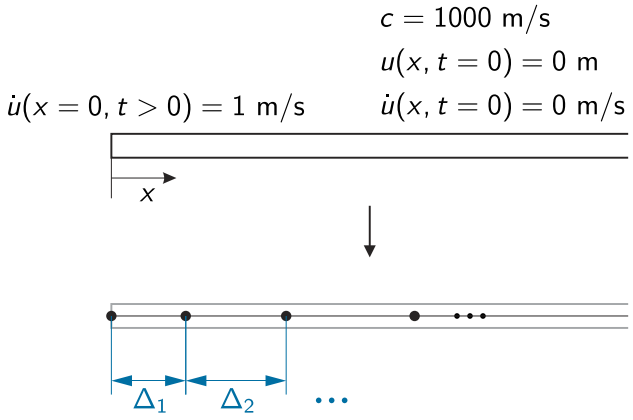

Fig. 7. 1D impact of an elastic bar problem: problem description and mesh used.

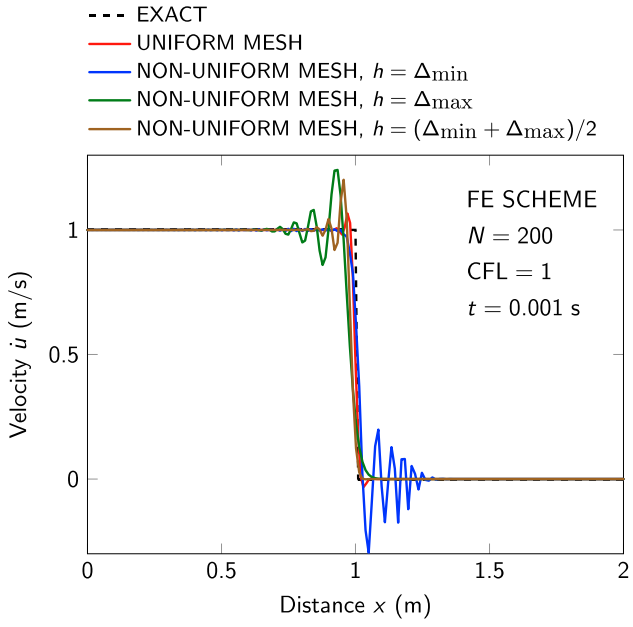

Fig. 8. Velocity distributions of the bar at $t = 0.001$ s calculated using FE scheme with the uniform and non-uniform meshes when CFL = 1; h denotes the element size used for the CFL number.

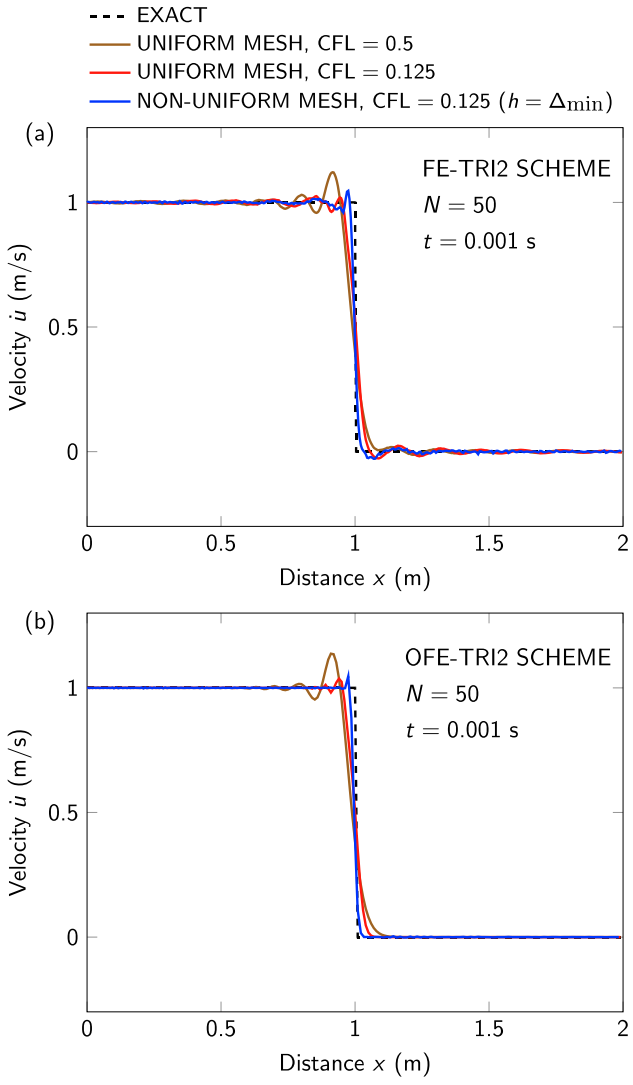

Fig. 9. Velocity distributions of the bar at $t = 0.001$ s calculated using (a) FE-TRI2 scheme and (b) OFE-TRI2 scheme with the uniform and non-uniform meshes; h denotes the element size used for the CFL number.

In all numerical examples, the waves do not reach the boundary of the computational domain for the time considered. We, therefore, do not use a technique such as a perfectly matched layer [25,29–32] to suppress artificially reflected waves at the boundary.

We also note that, as in the discussions given above, in all solutions we use the consistent mass matrices and for the evaluations of all matrices we use the Gaussian quadrature rules of sufficiently high order given in Ref. [33].

4.1. One-dimensional wave propagation

We consider the one-dimensional (1D) wave propagation due to an impact on an elastic semi-infinite bar, see Fig. 7. The displacement u is governed by the wave Eq. (4) with $c = 1000$ m/s, zero initial conditions and a unit step velocity applied at the left end of the bar. The computational domain $V = [0, 2]$ is considered and discretized with nodes spaced Δ_i, $i = 1, 2, \ldots$, apart as shown in Fig. 7. For the non-uniform mesh, we use

$$\Delta_i = \frac{\Delta_{\max} - \Delta_{\min}}{N-1}(i-1) + \Delta_{\min}, \quad i = 1, 2, \ldots, N \tag{26}$$

where $\Delta_{\max}$ and $\Delta_{\min}$ are the maximum and minimum distances between nodes, respectively, and N is the number of elements. In this problem we use $\Delta_{\max}/\Delta_{\min} = 4$.

We first solve the problem using the traditional two-node finite element with the Bathe time integration (denoted by FE scheme). In both uniform and non-uniform meshes, 200 elements are employed. Using a uniform mesh the best result is obtained when CFL = 1, see Ref. [34] and Fig. 8. Using the non-uniform mesh, however, this optimal CFL number cannot be achieved for all elements because each element has a different length. Fig. 8 shows the velocity distributions calculated using different element sizes to select the CFL number, namely with $h = \Delta_{\min}$, $h = \Delta_{\max}$ and $h = (\Delta_{\min} + \Delta_{\max})/2$. We see that depending on the element size used for the CFL number, spurious oscillations occur in front of or behind the wave front.

We then calculate the solutions using the FE-TRI2 and OFE-TRI2 schemes, with the second degree trigonometric functions. Using both the uniform and non-uniform meshes, the number of elements is equal to 50 and for the non-uniform mesh the CFL number is chosen using $h = \Delta_{\min}$. Fig. 9 gives the results where we see that quite accurate solutions are achieved with both schemes and the OFE-TRI2 scheme performs slightly better.

The monotonic convergence property, as the element sizes and the CFL number decrease, is very important when using a non-uniform mesh. If the smallest element size is used to select the CFL number, the other element sizes correspond to smaller CFL numbers, for which (using each element in a uniform mesh) with our scheme more accurate solutions are achieved. For this reason, we can expect that the OFE-TRI2 scheme accurately solves the problem using a non-uniform mesh with $h = \Delta_{\min}$ for the CFL number, see Fig. 9.

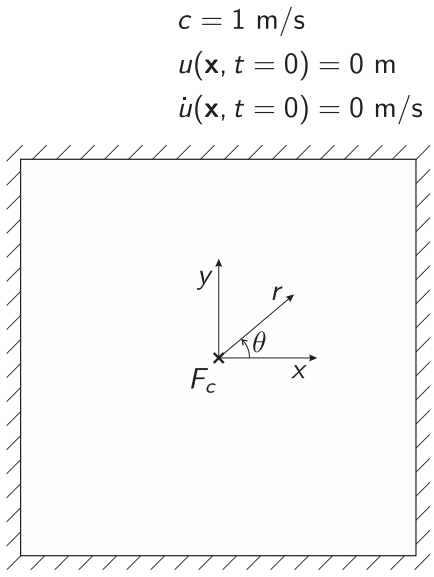

Fig. 10. Problem description of 2D scalar wave propagation in a pre-stressed membrane.

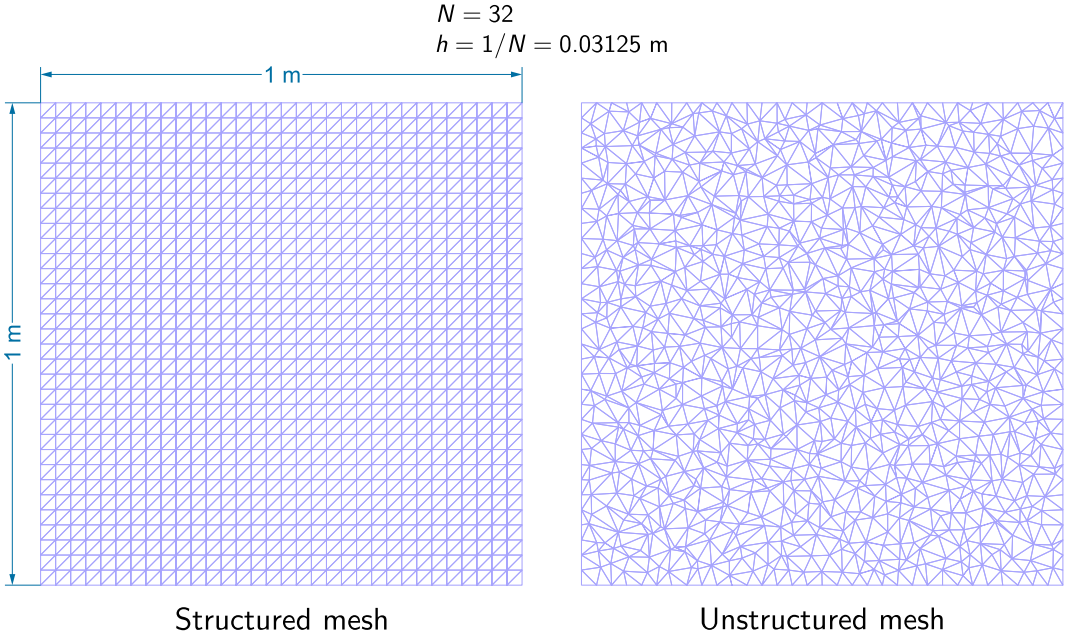

Fig. 11. Structured and unstructured meshes used for the 2D scalar wave propagation problem; N is the number of elements along each side.

4.2. Two-dimensional scalar wave propagation

We consider the two-dimensional (2D) scalar wave propagation due to a concentrated force (a point excitation) F_c at the center of a pre-stressed membrane, see Fig. 10, for which the transverse displacement u is governed by

$$\nabla^2 u + F_c(\mathbf{x} = \mathbf{0}, t) = \frac{1}{c^2}\frac{\partial^2 u}{\partial t^2} \tag{27}$$

with initial conditions

$$u(\mathbf{x}, t = 0) = 0\ \text{m}, \quad \dot{u}(\mathbf{x}, t = 0) = 0\ \text{m/s} \tag{28}$$

and the wave propagation velocity $c = 1$ m/s. Because of symmetry, we mesh only the domain $V = [0, 1] \times [0, 1]$ for the solution.

First, a Ricker wavelet [35] is considered as the concentrated force, which is defined as

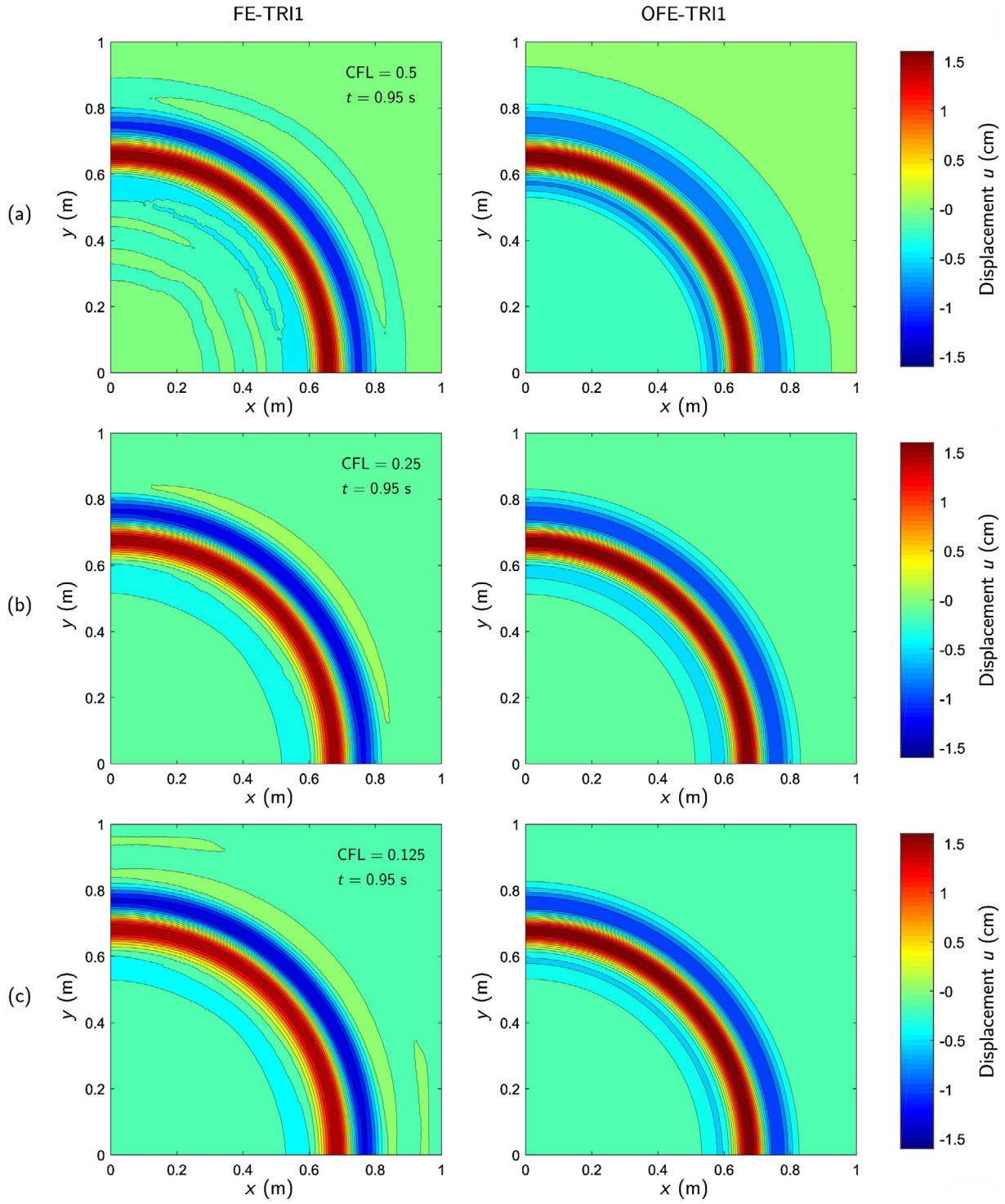

Fig. 12. Contour plots of displacement distributions of the membrane at $t = 0.95$ s calculated using FE-TRI1 scheme (left) and OFE-TRI1 scheme (right), both with the structured mesh ($h = 0.03125$ m): when (a) CFL = 0.5, (b) CFL = 0.25 and (c) CFL = 0.125.

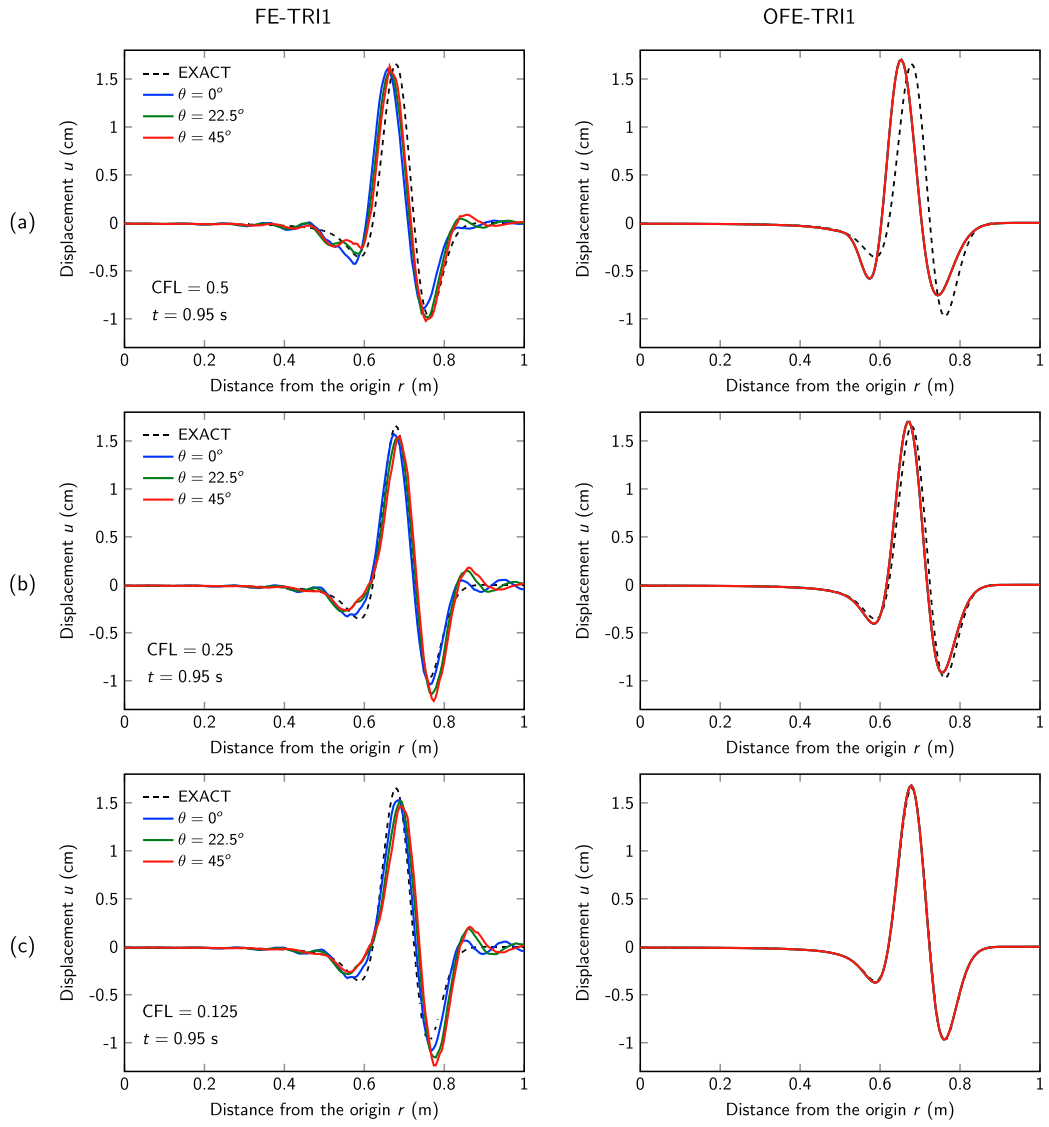

Fig. 13. Displacement distributions of the membrane along various directions ($\theta = 0^\circ, 22.5^\circ, 45^\circ$) at $t = 0.95$ s calculated using FE-TRI1 scheme (left) and OFE-TRI1 scheme (right), both with the structured mesh ($h = 0.03125$ m): when (a) CFL = 0.5, (b) CFL = 0.25 and (c) CFL = 0.125.

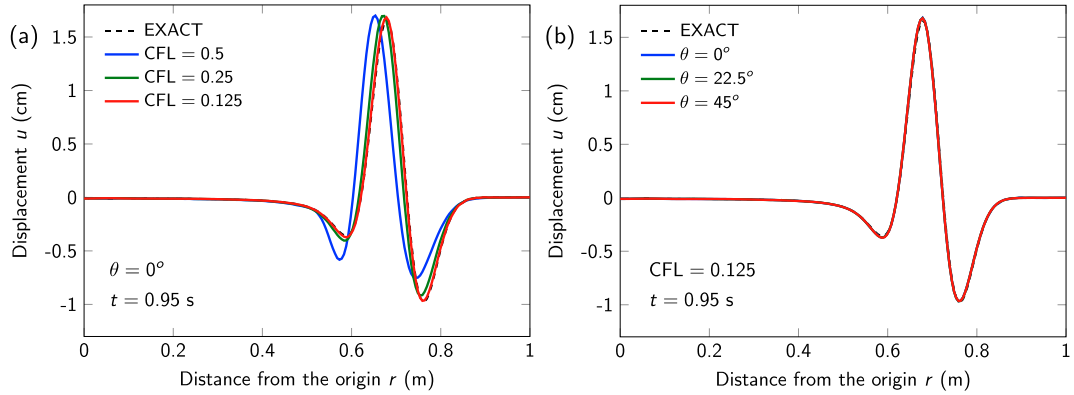

Fig. 14. Displacement distributions of the membrane at $t = 0.95$ s calculated using OFE-TRI1 with the unstructured mesh ($h = 0.03125$ m): (a) displacement distributions along horizontal axis with decreasing the CFL number and (b) displacement distributions along various directions when CFL = 0.125.

$$F_c = 0.4\left[1 - 2\pi^2 f_p^2 (t - t_s)^2\right] e^{-\pi^2 f_p^2 (t - t_s)^2} \tag{29}$$

where we use in this problem the peak frequency $f_p = 5$ Hz and the time shift $t_s = 0.25$ s. For the solution, we use the OFE-TRI1 scheme with the structured and unstructured meshes shown in Fig. 11 with the number of elements along each side $N = 32$ and the typical element size $h = 1/N = 0.03125$ m.

Figs. 12 and 13 show comparisons of the displacements calculated using the FE-TRI1 and the OFE-TRI1 schemes at $t = 0.95$ s using the structured mesh. We observe that the FE-TRI1 scheme does not give an accurate solution, whereas the solutions obtained using the OFE-TRI1 scheme converge monotonically to the exact solution as the CFL number decreases and are almost identical for any propagation angle θ considered.

In Fig. 14, we show the solutions using the OFE-TRI1 scheme with the unstructured mesh. As when using the structured mesh, we see that a more accurate solution is obtained with decreasing CFL number and the solution accuracy is practically independent of the propagation direction.

We next consider the concentrated force defined as

$$F_c = \begin{cases} 1.6 \times 10^2 t(0.1 - t) & \text{for } 0 \leqslant t < 0.1, \\ 0 & \text{for t } \geqslant 0.1. \end{cases} \tag{30}$$

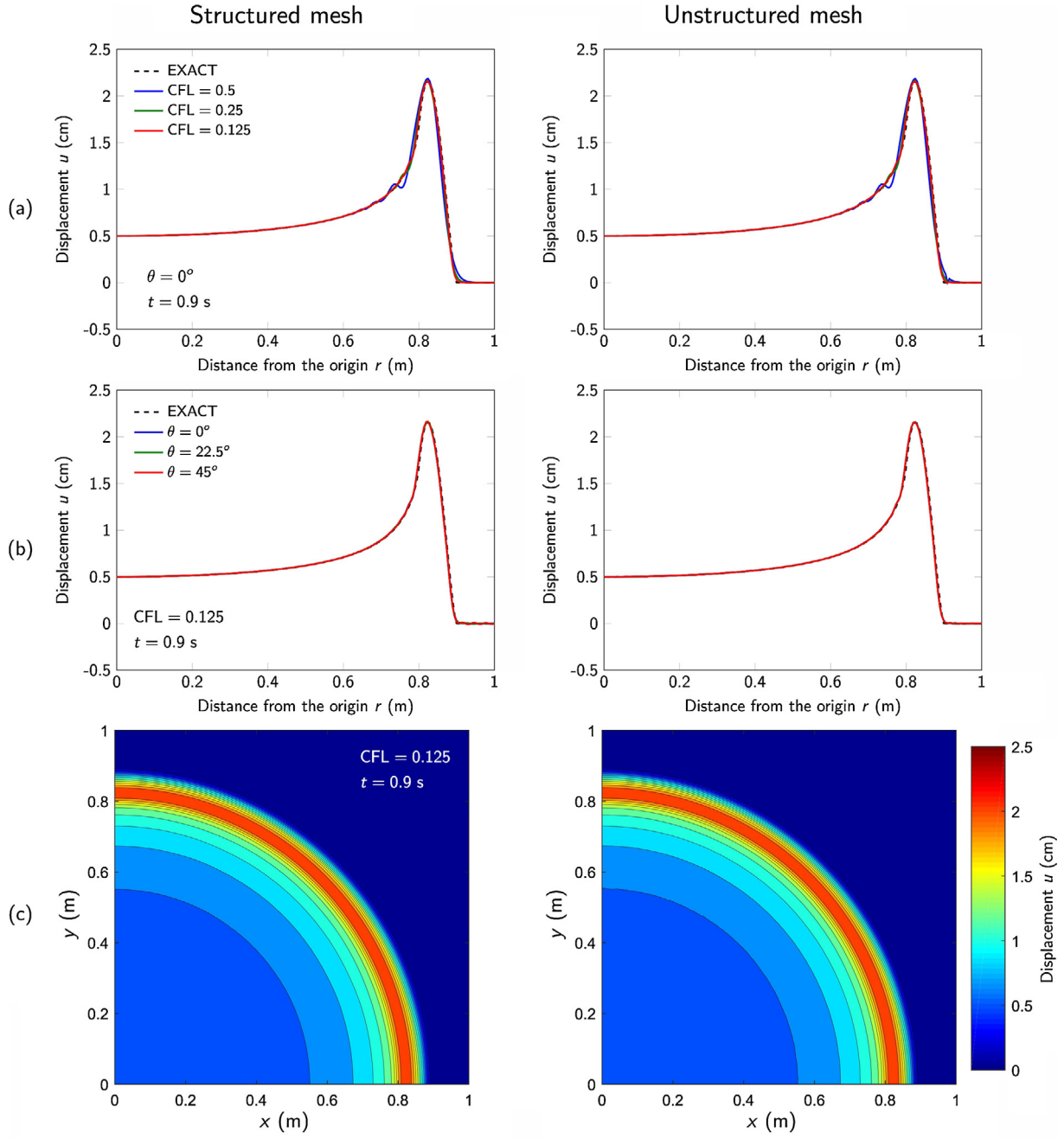

Fig. 15. Displacement distributions of the membrane at $t = 0.9$ s calculated using OFE-TRI1 scheme with the structured mesh (left) and with the unstructured mesh (right); in both cases $h = 0.015625$ m: (a) displacement distributions along horizontal axis with decreasing CFL number, (b) displacement distributions along various directions when CFL = 0.125 and (c) contour plots of displacement distributions when CFL = 0.125.

For this load case, we use the structured and unstructured meshes, both with $N = 64$ ($h = 0.015625$ m).

We compare the OFE-TRI1 solutions at $t = 0.9$ s using the structured mesh to those using the unstructured mesh, see Fig. 15. Here we again observe, like in the previous case, that using the structured mesh and unstructured mesh, the solution accuracy is improved as the CFL number decreases and the results for different propagation angles considered are almost the same.

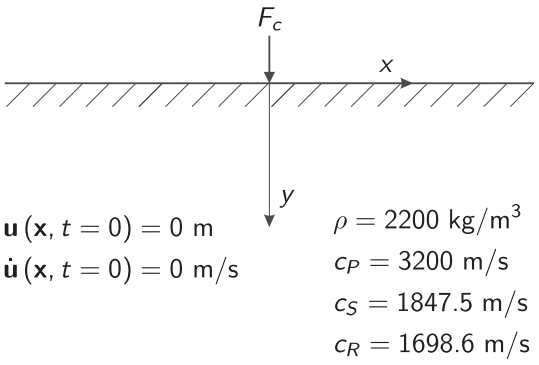

Fig. 16. Problem description of Lamb's problem [26] - 2D wave propagation in a plane strain elastic half-space.

4.3. Two-dimensional elastic wave propagation

We consider here the solution of the 2D waves propagating in a semi-infinite elastic medium in plane strain conditions [28], as described in Fig. 16. For the concentrated line force located at the free surface of the medium, we consider a Ricker wavelet, see Eq. (29), with the magnitude 2×10^6, $f_p = 10$ Hz and $t_s = 0.1$ s. The isotropic semi-infinite elastic medium has the mass density $\rho = 2200$ kg/m^3, the P-wave velocity $c_P = 3200$ m/s and the S-wave velocity $c_S = 1847.5$ m/s, which gives the Rayleigh wave velocity $c_R = 1698.6$ m/s. The initial displacements and velocities are zero and the computational domain $V = [0, 3200] \times [0, 3200]$ is considered with the structured and unstructured meshes shown in Fig. 11. This is a good test problem for a scheme to solve wave propagations, e.g. see Refs. [25,34].

We solve the problem using the OFE-TRI1 scheme with $N = 64$ ($h = 50$ m), and show the displacement histories at two receivers located at $\mathbf{x} = (640, 0)$ m and at $\mathbf{x} = (1280, 0)$ m in Figs. 17 and 18. The time step size Δt is calculated based on the P-wave velocity because the other types of waves are then also accurately predicted. As expected, in both cases, all waves are simulated more accurately as the CFL number is decreased.

To display the response predicted over the complete mesh, Fig. 19 shows the calculated von Mises stress distributions at $t = 1$ s using the meshes when CFL = 0.125.

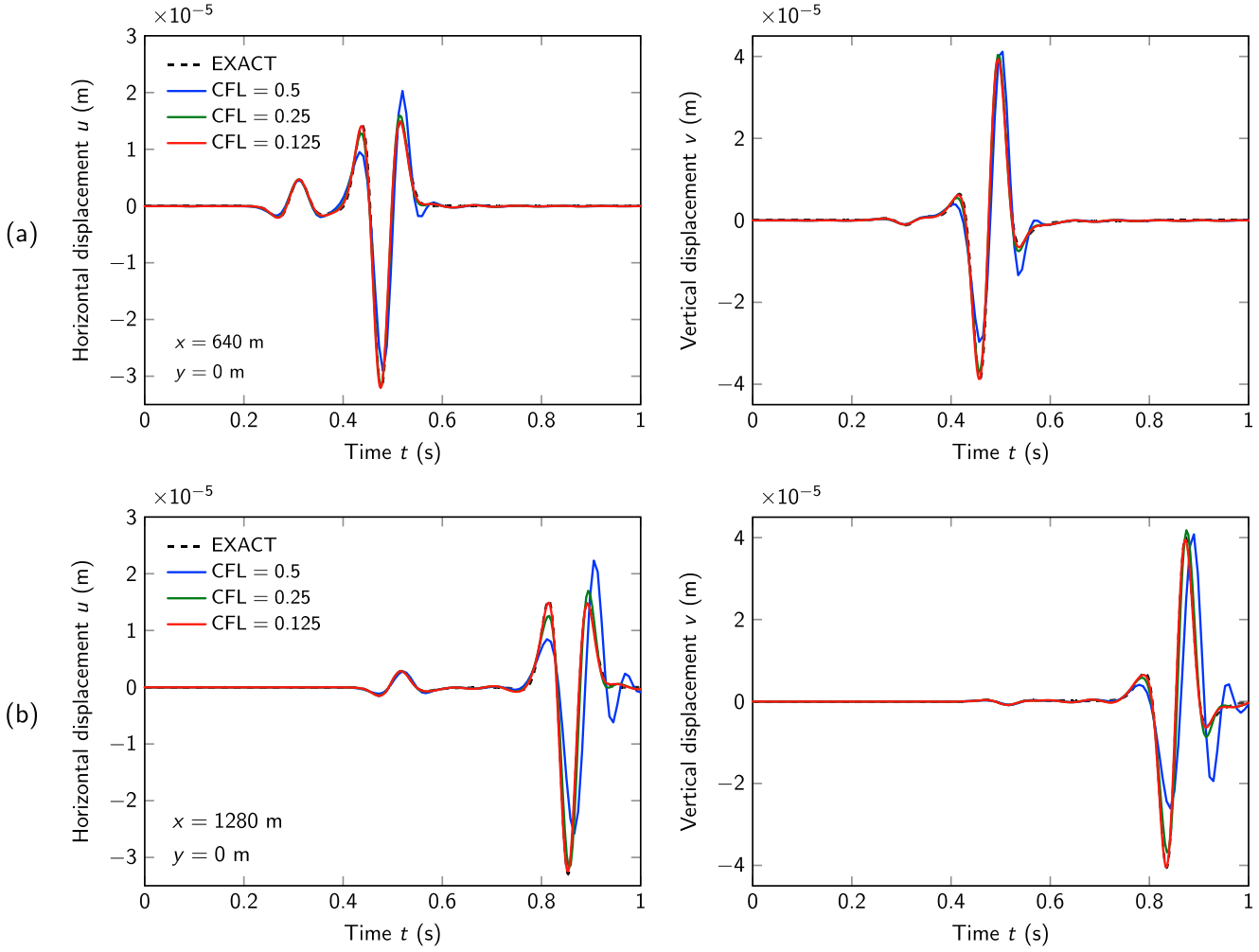

Fig. 17. Horizontal displacements (left) and vertical displacements (right) of the elastic medium calculated using OFE-TRI1 scheme with the structured mesh ($h = 50$ m): (a) displacement histories at $\mathbf{x} = (640, 0)$ m with decreasing CFL number and (b) displacement histories at $\mathbf{x} = (1280, 0)$ m with decreasing CFL number.

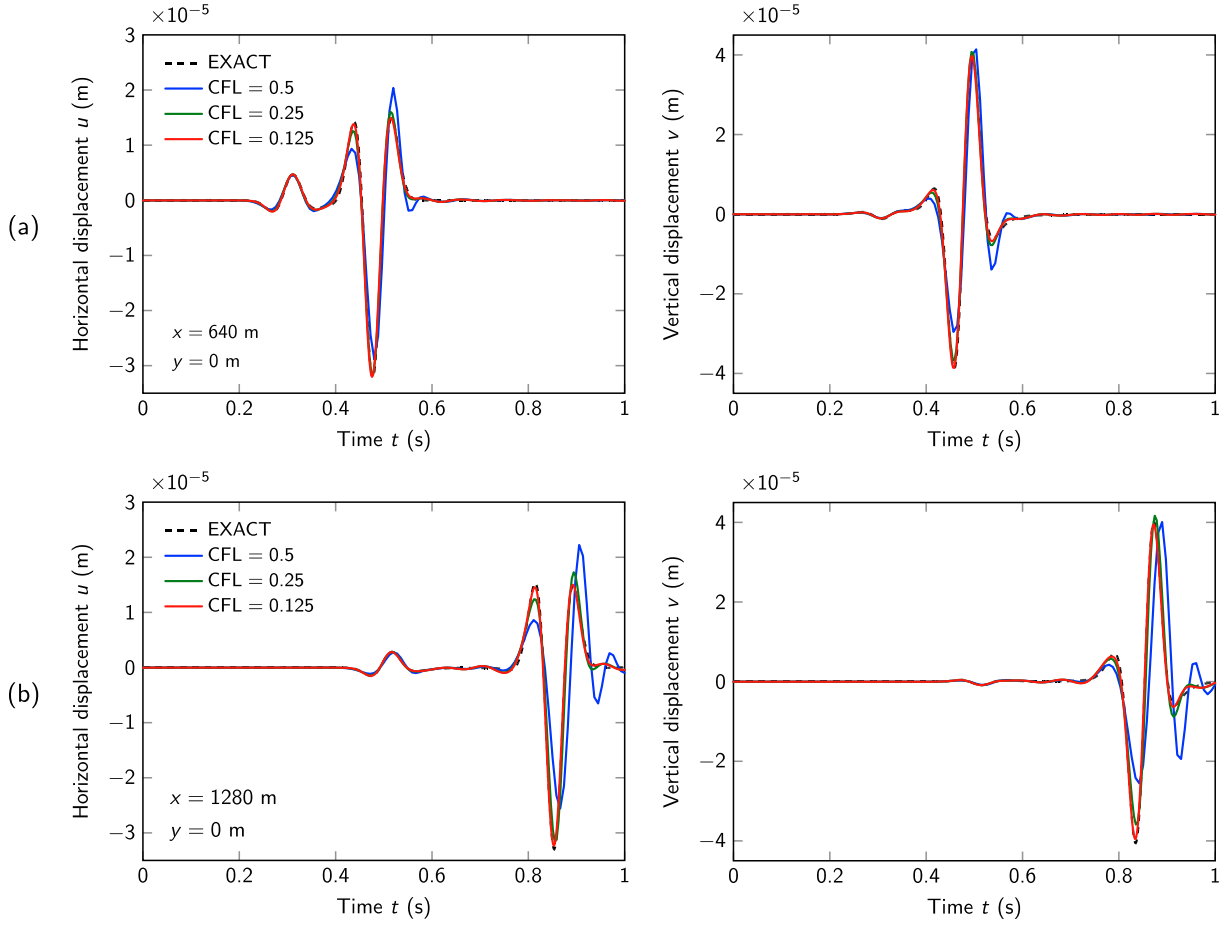

Fig. 18. Horizontal displacements (left) and vertical displacements (right) of the elastic medium calculated using OFE-TRI1 scheme with the unstructured mesh ($h = 50$ m): (a) displacement histories at $\mathbf{x} = (640, 0)$ m with decreasing CFL number and (b) displacement histories at $\mathbf{x} = (1280, 0)$ m with decreasing CFL number.

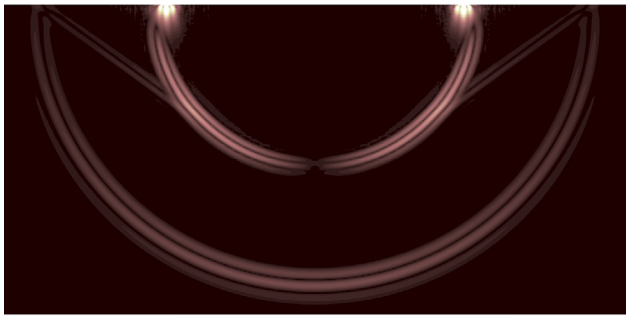

Fig. 19. Snapshots of von Mises stress distributions at $t = 1$ s calculated using OFE-TRI1 with the structured mesh (top) and with the unstructured mesh (bottom); in both cases $h = 50$ m and CFL = 0.125. Brighter color represents larger stress.

4.4. Two-dimensional wave propagation in a pre-stressed membrane with circular holes

We consider again the scalar wave propagation in the pre-stressed membrane but in this analysis, we have four circular holes, as shown in Fig. 20. The objective in this example is to show the performance of the OFE-TRI1 scheme when employed with the meshing scheme given in Refs. [20,21]. The problem needs to be solved for the excited wave, the transmitted wave and the reflected wave. The calculated wave profiles in the red and green directions in Fig. 20 are compared to a reference solution after the excited wave has passed the hole.

The meshing scheme consists of four steps, see Refs. [20,21]. In the first step the scheme immerses the pre-stressed membrane in a Cartesian grid with Δx and Δy as distances between lines. In the second step the boundaries are discretized with straight line segments Δs, during which geometry deficiencies are automatically removed. Thereafter, in the third step the scheme converts the internal cells into traditional finite elements. Finally, in the fourth step the scheme covers the empty space (region near the holes) with overlapping finite elements. Here for the wave propagation analysis, as shown in Fig. 20, all the traditional finite elements in the inner solution domain are also triangularized and converted to overlapping finite elements. In this example, we use $h = \Delta x = \Delta y = 0.02$ m and $\Delta s = 0.004\pi$ m.

We use a Ricker wavelet (29) with magnitude 0.4, $f_p = 10$ Hz and $t_s = 0.1$ s for the excitation force. The calculated solutions using the OFE-TRE1 scheme are compared with the reference

solution obtained using the OFE-TRI1 scheme with a very fine mesh of 28,055 elements.

Fig. 21 shows the calculated results after the wave passed the hole. We see that, as in the previous example solution, a decrease in the CFL number leads to a more accurate solution and that the wave profiles in the two directions ($\theta = 22.5^\circ$ and $\theta = 67.5^\circ$) are in good agreement with the reference solution. Some snapshots of calculated solutions at various observation times are shown in Fig. 22.

4.5. Solution times

We list here the computational times required to solve the two-dimensional example problems, in order to give some insight into the computational effort using the OFE-TRI1 scheme. A laptop with a single core Intel 2.40 GHz CPU and 24 GB RAM was used for calculating the solutions.

Table 1 presents the CPU times spent to obtain the solutions of the problems when using the OFE-TRI1 scheme with CFL = 0.125. It is seen that most of the computational effort is expended in the time integrations, as expected, and this effort depends on the total number of degrees of freedom, the mean half-bandwidth of the stiffness and mass matrices and the number of time steps. Hence, the use of higher degree trigonometric functions could lead to a more efficient solution because for a required accuracy a coarser mesh can be used. However, we recall that this approach may lead to ill-conditioning of the coefficient matrices [25].

5. Concluding remarks

The objective in this paper was to present an overlapping finite element enriched for transient wave propagation problems. We investigated the dispersion and dissipation properties and numerical anisotropy of the proposed overlapping finite element discretization used with the Bathe time integration method in two-dimensional solutions and illustrated these characteristics in regular and irregular meshes through the solutions of numerical examples.

The important property of the present scheme is that the use of a smaller CFL number leads to a more accurate solution

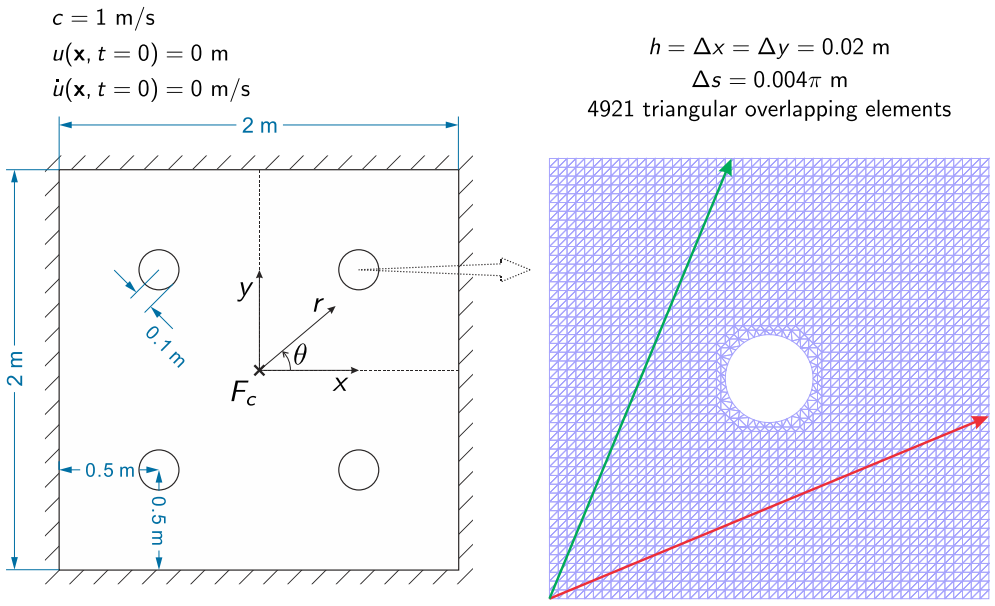

Fig. 20. 2D scalar wave propagation in a pre-stressed membrane: problem description and the mesh used; the line colored in red is the direction of $\theta = 22.5^\circ$ and the line colored in green is the direction of $\theta = 67.5^\circ$. (For interpretation of the references to color in this figure legend, the reader is referred to the web version of this article.)

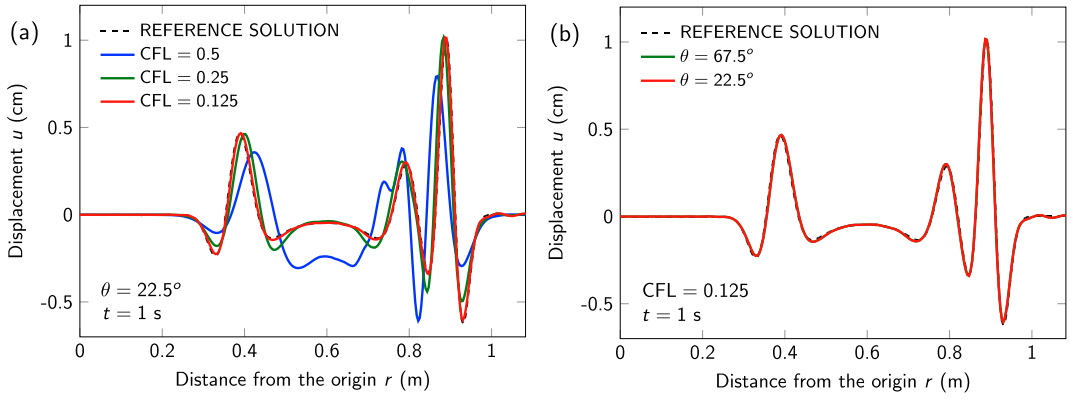

Fig. 21. Displacement distributions of the membrane with circular holes at $t = 1$ s calculated using OFE-TRI1 scheme: (a) displacement distributions along the direction of $\theta = 22.5^\circ$ with decreasing CFL number and (b) displacement distributions along the two directions ($\theta = 22.5^\circ$ and $\theta = 67.5^\circ$) when CFL = 0.125.

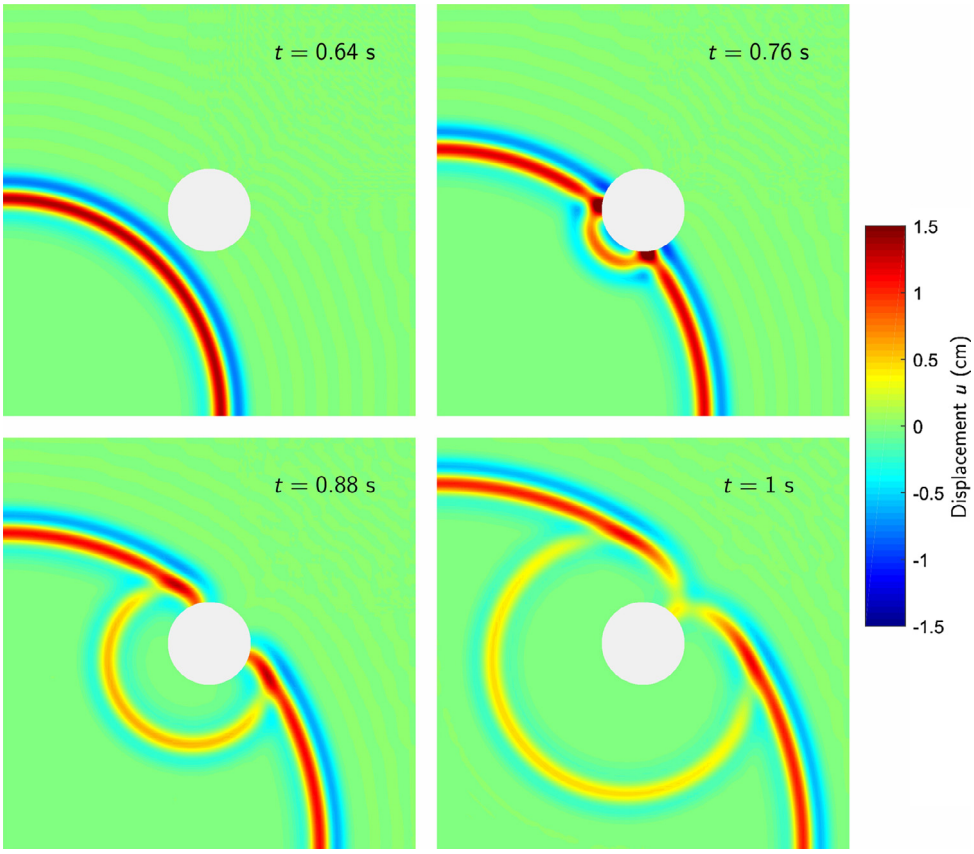

Fig. 22. Snapshots of displacement distributions of the membrane with circular holes at various observation times calculated using OFE-TRI1 scheme; CFL = 0.125.

Table 1
CPU times required to solve the two-dimensional example problems when using OFE-TRI1 scheme with CFL = 0.125.

Problem	Number of degrees of freedom	Mean half-bandwidth	CPU time (s) for constructing stiffness and mass matrices	CPU times (s) in the Bathe time integration		
				For initial calculations	For calculations in each time step (number of time steps)	For total calculation
Membrane	13,068	412	0.3	6.6	0.1 (243)	33.6
Semi-infinite elastic medium	50,700	811	3.9	103.7	0.8 (512)	499.2
Membrane with holes	31,020	844	0.6	73.8	0.5 (400)	274.4

irrespective of the propagation direction. Hence multiple types of waves propagating in different directions at different speeds can be accurately calculated at the same time by using the largest wave speed to select the CFL number.

These desirable solution characteristics have been observed even when using irregular meshes, which must often be employed in practical analysis. Given that the computational effort involved using the overlapping finite element is reasonable also when using irregular meshes, see Ref. [22], the proposed scheme shows much promise, including for use in the new solution paradigm of Refs. [20,21] when transient wave propagation problems need be solved.

While the cost of the numerical integrations of the element matrices was here only a small fraction of the total solution cost (see Table 1), a study to identify an optimal scheme for the numerical integration of the element matrices would be valuable.

The field of research considered in this paper is very large and important, in particular when general three-dimensional solutions are considered. But we can see that the avenue of using overlapping finite elements in direct time integrations (implicit or explicit integrations, see e.g. Ref. [36]) for the accurate solutions of general wave propagation problems, in linear and nonlinear analyses, with multiple waves traveling through anisotropic media is very promising.

References

[1] Krieg RD, Key SW. Transient shell response by numerical time integration. Int J Numer Meth Eng 1973;7:273–86.
[2] Belytschko T, Mullen R. On dispersive properties of finite element solutions. In: Miklowitz J, Achenbach JD, editors. Modern problems in elastic wave propagation. New York, NY: Wiley; 1978. p. 67–82.
[3] Mullen R, Belytschko T. Dispersion analysis of finite element semidiscretizations of the two-dimensional wave equation. Int J Numer Meth Eng 1982;18:11–29.
[4] Marfurt KJ. Accuracy of finite-difference and finite-element modeling of the scalar and elastic wave equations. Geophysics 1984;49:533–49.
[5] Abboud NN, Pinsky PM. Finite element dispersion analysis for the three-dimensional second-order scalar wave equation. Int J Numer Meth Eng 1992;35:1183–218.
[6] Thompson LL, Pinsky PM. A Galerkin least-squares finite element method for the two-dimensional Helmholtz equation. Int J Numer Meth Eng 1995;38:371–97.
[7] Deraemaeker A, Babuška I, Bouillard P. Dispersion and pollution of the FEM solution for the Helmholtz equation in one, two and three dimensions. Int J Numer Meth Eng 1999;46:471–99.

[8] Christon MA. The influence of the mass matrix on the dispersive nature of the semi-discrete, second-order wave equation. Comput Methods Appl Mech Eng 1999;173:147–66.
[9] Guddati MN, Yue B. Modified integration rules for reducing dispersion error in finite element methods. Comput Methods Appl Mech Eng 2004;193:275–87.
[10] Idesman AV, Schmidt M, Foley JR. Accurate finite element modeling of linear elastodynamics problems with the reduced dispersion error. Comput Mech 2011;47:555–72.
[11] Babuška I, Ihlenburg F, Paik ET, Sauter SA. A generalized finite element method for solving the Helmholtz equation in two dimensions with minimal pollution. Comput Methods Appl Mech Eng 1995;128:325–59.
[12] Franca LP, Farhat C, Macedo AP, Lesoinne M. Residual-free bubbles for the Helmholtz equation. Int J Numer Meth Eng 1997;40:4003–9.
[13] Patera AT. A spectral element method for fluid dynamics: Laminar flow in a channel expansion. J Comput Phys 1984;54:468–88.
[14] Seriani G, Oliveira SP. Dispersion analysis of spectral element methods for elastic wave propagation. Wave Motion 2008;45:729–44.
[15] Ham S, Lai B, Bathe KJ. The method of finite spheres for wave propagation problems. Comput Struct 2014;142:1–14.
[16] Kim KT, Bathe KJ. Transient implicit wave propagation dynamics with the method of finite spheres. Comput Struct 2016;173:50–60.
[17] De S, Bathe KJ. The method of finite spheres with improved numerical integration. Comput Struct 2001;79:2183–96.
[18] Lai B, Bathe KJ. The method of finite spheres in three-dimensional static analysis. Comput Struct 2016;173:161–73.
[19] Zhang L, Bathe KJ. Overlapping finite elements for a new paradigm of solution. Comput Struct 2017;187:64–76.
[20] Bathe KJ. The finite element method with "overlapping finite elements". In: Zingoni A, editor. proceedings sixth international conference on structural engineering, mechanics and computation – SEMC 2016, Cape Town, South Africa; 2016.
[21] Bathe KJ, Zhang L. The finite element method with overlapping elements – A new paradigm for CAD driven simulations. Comput Struct 2017;182:526–39.
[22] Zhang L, Kim KT, Bathe KJ. The new paradigm of finite element solutions in CAD – Computational efficiency of the procedure. Comput Struct, in press.
[23] Bathe KJ. Conserving energy and momentum in nonlinear dynamics: a simple implicit time integration scheme. Comput Struct 2007;85:437–45.
[24] Bathe KJ, Noh G. Insight into an implicit time integration scheme for structural dynamics. Comput Struct 2012;98–99:1–6.
[25] Ham S, Bathe KJ. A finite element method enriched for wave propagation problems. Comput Struct 2012;94–95:1–12.
[26] Bathe KJ. Finite element procedures. Second ed. Watertown, MA: Klaus-Jürgen Bathe; 2014. Higher Education Press, China; 2016.
[27] Kohno H, Bathe KJ, Wright JC. A finite element procedure for multiscale wave equations with application to plasma waves. Comput Struct 2010;88:87–94.
[28] Lamb H. On the propagation of tremors over the surface of an elastic solid. Philos Trans Roy Soc Lond Series A, Containing Pap Math Phys Character 1904;203:1–42.
[29] Berenger JP. A perfectly matched layer for the absorption of electromagnetic waves. J Comput Phys 1994;114:185–200.
[30] Chew WC, Weedon WH. A 3D perfectly matched medium from modified maxwell's equations with stretched coordinates. Microwave Opt Technol Lett 1994;7:599–604.
[31] Teixeira FL, Chew WC. General closed-form PML constitutive tensors to match arbitrary bianisotropic and dispersive linear media. IEEE Microwave Guided Wave Lett 1998;8:223–5.
[32] Sacks ZS, Kingsland DM, Lee R, Lee JF. A perfectly matched anisotropic absorber for use as an absorbing boundary condition. IEEE Trans Antennas Propag 1995;43:1460–3.
[33] Dunavant DA. High degree efficient symmetrical Gaussian quadrature rules for the triangle. Int J Numer Meth Eng 1985;21:1129–48.
[34] Noh G, Ham S, Bathe KJ. Performance of an implicit time integration scheme in the analysis of wave propagations. Comput Struct 2013;123:93–105.
[35] Ricker N. The form and laws of propagation of seismic wavelets. Geophysics 1953;18:10–40.
[36] Noh G, Bathe KJ. An explicit time integration scheme for the analysis of wave propagations. Comput Struct 2013;129:178–93.